J Mater Sci (2007) 42:1269–1278
DOI 10.1007/s10853-006-1394-8

Elastic properties of powders during compaction. Part 2: elastic anisotropy

M. L. Hentschel · N. W. Page

Received: 22 July 2004 / Accepted: 2 October 2005 / Published online: 26 January 2007

Abstract Isotropy in the elastic properties of powders undergoing uniaxial compaction in a cylindrical die was evaluated from in situ measurements of elastic wave speed. Shear and bulk longitudinal wave speeds were measured in both the axial (pressing) and radial directions. For the five different metal powders studied, wave speeds were generally higher in the axial direction. As such, the powder body was best described as a transversely isotropic material; complete isotropy was approached only when the powder was close to the loose packed state, or completely solid. Transversely isotropic elastic moduli analogous to the common isotropic 'engineering' moduli (Young's modulus, Poisson's ratio, etc.) were calculated by combining elastic wave speed measurements with the Saint-Venant approximation. Pseudo-isotropic elastic moduli (calculated from axial wave speed measurements and assuming elastic isotropy) were found to be only qualitatively similar to transversely isotropic elastic moduli for the axial plane.

Introduction

Results on the evolving elastic moduli of powders during uniaxial compaction have been discussed in a companion paper (Hentschel and Page submitted). These elastic moduli were calculated from in situ measurements of bulk longitudinal and shear elastic wave speeds for propagation in the axial (pressing) direction. Elastic properties of the powder compact were characterised by the isotropic moduli Young's modulus (E), and Poisson's ratio (v), calculated from the elastic wave speeds according to Eqs. 1 and 2.

$$E = \rho c_S^2 \frac{3c_L^2 - 4c_S^2}{c_L^2 - c_S^2} \tag{1}$$

$$v = \frac{c_L^2 - 2c_S^2}{2(c_L^2 - c_S^2)} \tag{2}$$

where ρ, density; and c_L, c_S are bulk longitudinal, and shear elastic wave speeds respectively.

These equations assume the propagating medium is homogeneous, linearly elastic, and isotropic. The validity of these assumptions for a powder undergoing uniaxial compaction is considered in greater detail in the following.

Homogeneity

Homogeneity of a powder compact requires uniform distribution of constituent solid phase materials. Even for the case of powders comprised of only a single solid phase material, inhomogeneities arise simply as density variations throughout the compact. Minimising such density variations is often critical, as strength, and rate of sintering depend strongly on density [1]. Thus, low density regions of powder compacts may be more prone to failure, or sinter at a slower rate distorting component shape [2].

As the density of a powder body is intimately linked to its stress history, non-uniform density implies a

M. L. Hentschel · N. W. Page (✉)
Mechanical Engineering, The University of Newcastle, Newcastle, NSW 2308, Australia
e-mail: npage2@telstra.com

corresponding non-uniformity in stress. One such source of non-uniform stress is friction between the powder and containment surfaces. Die wall friction opposes the applied load, effectively transferring part of the compaction force to the die walls and producing stress and density gradients within the compact. Spatial variation of density is typically quite complex [1–6], depending on the coefficient of friction for the powder-die wall interface, stress bifurcation abilities of the powder (coefficient of lateral pressure), and compact aspect ratio (quotient of height by diameter). A reduction in any of these parameters generally serves to decrease density variations. For a given powder (fixed coefficient of lateral pressure) effects of die wall friction can be minimised by lubrication, or reducing the compact aspect ratio. Compaction geometry is also important. For example, uniaxial compaction in an unsupported ('floating') die ensures the force transmitted to the lower punch is equal to the applied compaction force, which effectively reduces the compact aspect ratio by half [5, 6].

Superimposed upon stress gradients due to die wall friction are heterogeneous stresses which arise from non-uniformities in particle packing; a result of variations in particle size and shape. When an external force is applied to a non-uniform packing, the majority of the applied load is supported by a relatively small number of the possible paths through the powder, forming so-called 'force chains' (e.g. [7]). As a result some powder particles (those within force chains) experience relatively high stresses, while others remain virtually stress-free. In a powder undergoing significant compaction, this contribution to stress heterogeneity is unlikely to dominate gradients induced by die wall friction, as appreciable densification requires permanent deformation of the particles (fracture, plastic flow, etc.). Such deformation will occur preferentially in regions of highest stress, serving to reduce local forces. Thus, force chains would repeatedly break and reform during compaction, minimising their ability to contribute significantly to density variations throughout the compact.

Few studies describing effects of density variations on elastic properties have been reported. Rice and Donahue [8] considered the effects of inhomogeneous density on the elastic properties of porous materials by evaluating Young's modulus according to a selection of models applicable to composite materials. Within these models, the bulk was considered as a composite of two different 'materials' with different densities or porosity type. It was concluded that, unless the inhomogeneity is particularly severe, the influence on elastic properties is minimal.

This is supported by experimental measurements of elastic wave speeds in powders during compaction. Dawson et al. [9] measured bulk longitudinal wave speeds in iron powder undergoing uniaxial compaction. No appreciable difference was found in bulk longitudinal wave speed (hence elastic properties) for compacts with final aspect ratios between approximately 0.16–0.22. Likewise, in the study which forms the basis of this work [10], shear and bulk longitudinal wave speeds were measured as a function of porosity in both stainless steel and copper powders. Again these were each consistent for compacts with markedly different final aspect ratios (ranging from 0.12 to 0.46). Density distributions were not measured, however the good agreement between wave speeds indicates either density gradients were negligible, or wave speeds (hence elastic properties) are relatively insensitive to the prevailing inhomogeneities in density. Neither scenario precludes the use of Eqs. 1 and 2 in the present case.

Linear elastic response

The second assumption to be examined is whether the compact may be regarded as a linearly elastic medium. Equations 1 and 2 are essentially a combination of Hooke's law and Newton's second law of motion (e.g. [11]). Hooke's law requires deformation to be (i) elastic (deformation is completely recoverable), and (ii) linear (elastic strain components are directly proportional to corresponding stress components). Both assumptions must be satisfied for Eqs. 1 and 2 to be valid.

Powder compacts at densities close to that of the solid phase would satisfy both criteria; provided the solid phase is itself a linear elastic material. However, it is not obvious whether this still holds at the lowest densities when the bulk response is dominated by inter-particle contact mechanics. Analysis of the stiffness between two contacting bodies generally predicts non-linear load-deflection behaviour (e.g. [12–14]). Further, it has also been argued [15] that internal yield (failure of some inter-particle contacts) can be expected for finite changes in applied stress. Either will likely invalidate the assumption of bulk linear elastic response for elastic moduli measured from large changes in applied stress (as traditional quasi-static methods require).

However a strong positive of measuring elastic properties by wave propagation techniques is that Eqs. 1 and 2 are derived assuming infinitesimally small stress increments. Thus, the assumption of a linear

elastic response need only hold over a relatively small range of stresses (wave amplitude), and the strength of inter-particle contacts need only be very small. In the present work, with elastic wave speeds calculated from the measured propagation time of ultrasonic pulses, this condition should be well satisfied. For instance, Matikas et al. [16] quote material displacements induced by the passage of the ultrasound to be of the order of 10^{-10} m.

Experiments have been conducted [10] to test whether ultrasonic pulse propagation produced a measurable effect on powder density (i.e. yield) under conditions relevant to this study. This was achieved by monitoring the density of a powder sample subject to the minimum applied pressure at which wave speeds were measured in this study (0.06 MPa). Powder thickness (density) was measured, initially (for 25 min) without ultrasound propagating through the powder, then for a further time (75 min, with a pulse repetition frequency of 5 kHz) with ultrasonic pulse propagation. No difference between the two situations was apparent, indicating the passage ultrasound did not induce discernible density changes (internal yield) in the powder body. Hence, it is felt that the assumption of linear elasticity inherent in Eqs. 1 and 2 is valid for the experimental configuration used here (further details are provided below, and elsewhere [10]).

Elastic isotropy

Often a uniaxially compacted powder is assumed to be isotropic. In many cases, this assumption is implicitly invoked by using isotropic parameters to describe the compacted powder (e.g. [17–23]). However, uniaxial powder compaction in a rigid die is an inherently anisotropic process (e.g. [1, 22, 24]). Viewed as a continuum, axial deformation will usually far exceed deformation in the radial direction, which is constrained by the die walls. On this basis it is likely that the pore structure, and hence those physical properties dependent on the nature of porosity, will display directional dependence [24–26]. This calls into question the assumption of isotropy mechanical properties, including elastic properties.

Shima and Saleh [27] investigated anisotropy in powders biaxially compacted at various relative strain rates. Their experimental data clearly demonstrates anisotropy may be induced in a powder which is subjected to compacting stresses that are not equal in all directions, as is the case for uniaxial compaction in a rigid cylindrical die. Compaction-induced anisotropy is also suggested to cause corresponding anisotropies in the properties of sintered powder compacts, most evident as differential shrinkage (e.g. [27–29]).

Several authors have reported results relevant to the specific case of elastic isotropy in compacted powders and porous materials [30–36]. This has often been performed by evaluating whether longitudinal wave speed through the sample has directional dependence. Alternatively, isotropy about a particular direction (axis) can also be detected by rotating the polarisation of the shear wave displacement vector [36]. The shear wave speed will change depending on the stiffness of the material plane in which the shear wave displacement vector oscillates. A variety of results have been obtained on the nature of elastic isotropy: Brettell [35] found longitudinal wave speed was up to 11% higher in the pressing direction than in the directions perpendicular, while others report the converse [33, 34]. Martin et al. [30] found virtually no difference with propagation direction, while Parthasarathi and Prucher [31] produced samples that display both types of behaviour.

Inconsistencies in the nature of compaction-induced elastic anisotropy may possibly arise from differences in compaction techniques, or the particular mix of compaction and sintering to which some samples were subjected. Similar inconsistencies have been explained [29] for differences in the observed nature of shrinkage anisotropy of sintered powder compacts. It is also possible that anisotropy of bulk elastic properties may be influenced by anisotropic characteristics of the starting powders, particularly non-isometric particle shape, or preferred orientation of a crystalline direction in solid phase material which itself has strong elastic anisotropy. For instance, Krzesińska et al. [32] have described a study of a graphite powder during compaction, for which bulk elastic anisotropy was partially attributable to compaction-induced preferential alignment of the graphite crystalline axes.

Importantly though, the demonstrated difference in longitudinal elastic wave speeds with direction, indicates that elastic isotropy may not be realised for compacted powders. Should this be the case, Eqs. 1 and 2 would no longer be applicable, and additional elastic moduli are required to describe the elastic behaviour of compacted powders. For sample production methods which are symmetric about an axis (e.g. uniaxial compaction in a cylindrical die), it is most likely the compact will exhibit *transverse isotropy* [31, 34, 36], with elastic properties that are identical in radial directions, but distinct from those in the axial direction. This is considered in detail in the current work.

Transverse isotropy

Throughout the following, it is assumed that the transversely isotropic material has cylindrical geometry, with the unique axis collinear to the cylinder axis (3) of a Cartesian coordinate system (1, 2, 3). As material properties are identical for all directions within the radial (1, 2) plane, it is also assumed that waves propagating in the radial direction do so along the 1-axis (to simplify notation). Of course, neither assumption is necessary; however, as this is the prevailing geometry for uniaxial powder compaction in a cylindrical die, it simplifies description and allows ready interpretation in terms of the compact geometry.

For a medium in which body forces can be neglected, the most general form of Hooke's law is given by Eq. 3.

$$\sigma_i = C_{ij}\varepsilon_j \tag{3}$$

where σ and ε are stress and strain components respectively, C is the stiffness matrix. $i, j = 1, \ldots, 6$ using the contracted notation.

For an isotropic material, the stiffness matrix, C_{ij}, has 12 non-zero components between which the following relations hold:

$$\begin{aligned} &C_{11} = C_{22} = C_{33} \\ &C_{44} = C_{55} = C_{66} \\ &\text{with } C_{12} = C_{13} = C_{23} = C_{21} = C_{31} = C_{32} = (C_{11} - 2C_{44}) \end{aligned} \tag{3a}$$

These can be expressed in terms of the more common 'engineering' elastic moduli, by defining the Lamé constants, λ and μ as: $\lambda = C_{12}$ and $\mu = C_{44}$.

For a transversely isotropic material, the stiffness matrix also has 12 non-zero components. However, due to reduced symmetry relative to the isotropic case, the number of independent components (elastic moduli) increases to five. The following relations hold between these components (e.g. [38]):

$$\begin{aligned} &C_{11} = C_{22} \\ &C_{12} = C_{21} \\ &C_{13} = C_{23} = C_{32} = C_{31} \\ &C_{33} \\ &C_{44} = C_{55} \\ &\text{with } C_{66} = \frac{1}{2}(C_{11} - C_{12}) \end{aligned} \tag{3b}$$

As with the isotropic case, elastic wave speed measurements can be used to determine the elastic moduli of a transversely isotropic material, with the addition that wave propagation direction must also be considered. Relations between elastic moduli of a transversely isotropic material and the shear and longitudinal elastic wave speeds in two principal directions (3, 1) are given in Table 1 (e.g. [38]).

Hence, measurement of these four unique wave speeds allows four of the five elastic moduli (C_{11}, C_{12}, C_{33}, C_{44}) to be determined. For the remaining elastic modulus C_{13}, wave speeds must be measured in a third (non-orthogonal) direction. Such measurements pose considerable technical challenges, and hence, were not performed in this work.

To distinguish between the two cases, the following equalities may be evaluated. These will hold for complete isotropy, but not for transverse isotropy (Eq. 3a, b) and Table 1).

$$c_{L,r} = c_{L,a} \quad \text{or} \quad C_{11} = C_{33}$$

$$c_{S,rr} = c_{S,ra} = c_{S,a} \quad \text{or} \quad C_{44} = \frac{1}{2}(C_{11} - C_{12})$$

A further equality that will hold for either transverse or complete isotropy is:

$$c_{S,rr} = c_{S,a} \quad \text{or} \quad C_{44,\text{axial}} = C_{44,\text{radial}}$$

Table 1 Relations between wave speed and elastic moduli for a transversely isotropic medium

Propagation mode	Propagation direction	Wave displacement vector	Wave speed
Longitudinal	Axial (3)	Axial (3)	$c_{L,a} = \sqrt{C_{33}/\rho}$
Shear	Axial (3)	Any direction in radial (1, 2) plane	$c_{S,a} = \sqrt{C_{44}/\rho}$
Longitudinal	Radial (1)	Radial (1)	$c_{L,r} = \sqrt{C_{11}/\rho}$
Shear	Radial (1)	Radial (2)	$c_{S,rr} = \sqrt{C_{44}/\rho}$
Shear	Radial (1)	Axial (3)	$c_{S,ra} = \sqrt{(C_{11} - C_{12})/2\rho}$

ρ is bulk density. Wave speeds are labelled according to propagation mode (first subscript), propagation direction (second subscript), and polarisation direction (third subscript) where appropriate. Hence, $c_{S,ra}$ denotes a shear wave propagating in the radial direction, polarised in the axial direction. Polarisation need not be specified for shear waves propagating in the axial direction, as all radial directions are equivalent

Thus, three ratios may be defined to quantify the anisotropy of a transversely isotropic material:

$$A_1 = \frac{C_{44,\text{axial}}}{C_{44,\text{radial}}} = \left(\frac{c_{S,a}}{c_{S,rr}}\right)^2 \quad (4)$$

$$A_2 = \frac{C_{33}}{C_{11}} = \left(\frac{c_{L,a}}{c_{L,r}}\right)^2 \quad (5)$$

$$A_3 = \frac{2C_{44}}{C_{11} - C_{12}} = \left(\frac{c_{S,a}}{c_{S,ra}}\right)^2 \quad (6)$$

A_1 is useful for evaluating whether a medium is either transversely or completely isotropic. A_2 and A_3 distinguish between the two, quantifying compressive anisotropy and shear anisotropy respectively.

Experimental methods

Five different powders (Table 2) were each uniaxially compacted within a rigid cylindrical die using applied pressures up to 560 MPa. Shear and longitudinal ultrasonic transducers were used to measure elastic wave speeds in situ for propagation in the axial (pressing) and radial directions (see also [10]). Comparison between results for the five powders allows the effects of solid phase material, and particle shape on elastic properties to be evaluated, analogous to pseudo-isotropic elastic moduli calculated from axial wave speed measurements considered elsewhere [Hentschel and Page submitted, 10].

Results and discussion

Axial and radial wave speeds in the spheroidal copper powder as a function of compact porosity are presented in Fig. 1. As results for the remaining powders were found to be qualitatively similar, some general observations are made on the basis of this figure.

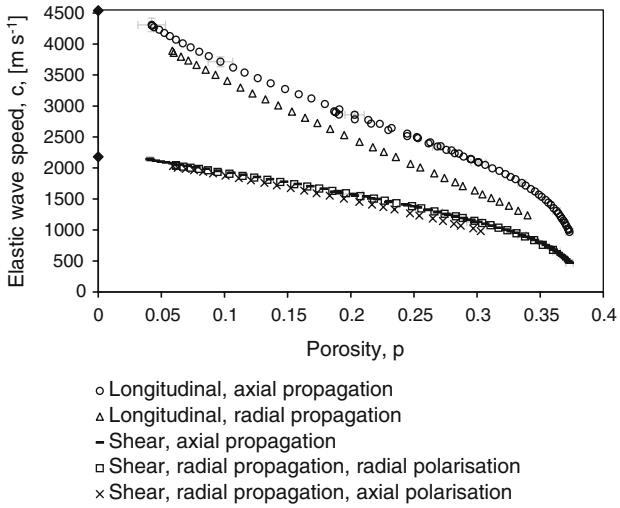

Fig. 1 Porosity dependence of elastic wave speeds measured in situ during uniaxial compaction of spheroidal copper powder. (○) Longitudinal wave speed for propagation in the axial direction. (Δ) Longitudinal wave speed for propagation in the radial direction. (–) Shear wave speed for propagation in the axial direction with polarisation in the radial plane. (□) Shear wave speed for propagation in the radial direction with polarisation in the radial plane. (×) Shear wave speed for propagation in the radial direction with polarisation in the axial plane. The filled diamonds are shear and bulk longitudinal elastic wave speeds in (isotropic) solid copper

- Radial shear wave speeds with polarisation in the radial direction agree closely with axial shear wave speeds over the common porosity range $(c_{S,rr} \approx c_{S,a})$.
- Axial longitudinal wave speed exceeds radial longitudinal wave speed $(c_{L,a} > c_{L,r})$.
- Axial shear wave speed slightly exceeds radial shear wave speed with polarisation in the axial direction $(c_{S,a} \approx c_{S,rr} > c_{S,ra})$..

Table 2 Powder details

Powder	Particle shape[a]	Comparative purpose in testing schedule	Shape descriptors[b]	
			AR	$\sqrt{FF}$
A. Dendritic copper	Dendritic	Particle shape (B, C)	0.605	0.796
B. Irregular copper[c]	Irregular	Particle shape (A, C)	0.717	0.822
C. Spheroidal copper	Spheroidal	Solid phase material properties (D, E)	0.934	0.994
D. Stainless steel	Spheroidal	Solid phase material properties (C, E)	0.843	0.957
E. Aluminium	Spheroidal	Solid phase material properties (C, D)	0.773	0.931

Micrographs illustrating particle shape are presented elsewhere [10, Hentschel and Page submitted]

[a] Terminology of British Standard 5600

[b] Defined in Eqs. 1 and 2 in Hentschel and Page (submitted)

[c] Denoted *Irregular copper (MM)* in Hentschel and Page (submitted)

- As porosity decreases, both radial wave speeds approach the corresponding axial wave speeds.
- At the highest porosities, the axial and radial longitudinal wave speeds appear to be converging.

These points embody four important results.

1. The difference between radial and axial wave speeds demonstrates powders exhibit elastic anisotropy during uniaxial compaction.
2. Agreement between $c_{S,\ a}$ and $c_{S,\ rr}$ is consistent with a transversely isotropic medium.
3. Longitudinal wave speeds differ most. This suggests much of the elastic anisotropy is attributable to differences in compressive stiffness between axial and radial directions: shear stiffness in the radial direction is only slightly lower than its axial counterpart.
4. Elastic anisotropy is most pronounced mid-way through compaction. Axial and radial longitudinal wave speeds appear to be converging at either end of the measured porosity range.

This final point suggests isotropy is approached when the compact is either close to the solid phase density, or only lightly consolidated (note $p = 0.37$ corresponds to the 'tapped' density state of the spheroidal copper powder in Fig. 1). Given the particles themselves are approximately isometric, it is expected the porosity within the undeformed array of particles will also be isotropic, and hence any porosity dependent properties likewise. This is unable to be rigorously tested with the present apparatus though, as the ultrasonic pulses are strongly attenuated at high porosities. At the other extreme, as porosity is reduced towards zero, re-convergence towards isotropy is likely due to the pores becoming increasingly spherical (to reduce local stresses) as solid phase density is approached.

These observations on the progression of anisotropy are quantified by use of the ratios defined in Eqs. 4–6. Calculated values of these ratios as a function of compact porosity are presented in Fig. 2.

Figure 2a demonstrates generally good agreement between $C_{44,\ \mathrm{radial}}$ and $C_{44,\ \mathrm{axial}}$ (C_{44} calculated from $c_{S,\ rr}$, and $c_{S,\ a}$ respectively). Excepting low porosity data for the dendritic copper powder, the difference is less than 5%. For the dendritic powder, the maximum difference is 12%. It is felt this discrepancy was most likely due to a slight mis-alignment of the shear polarisation direction with the radial direction, so the plane in which shear oscillation occurred for the radial

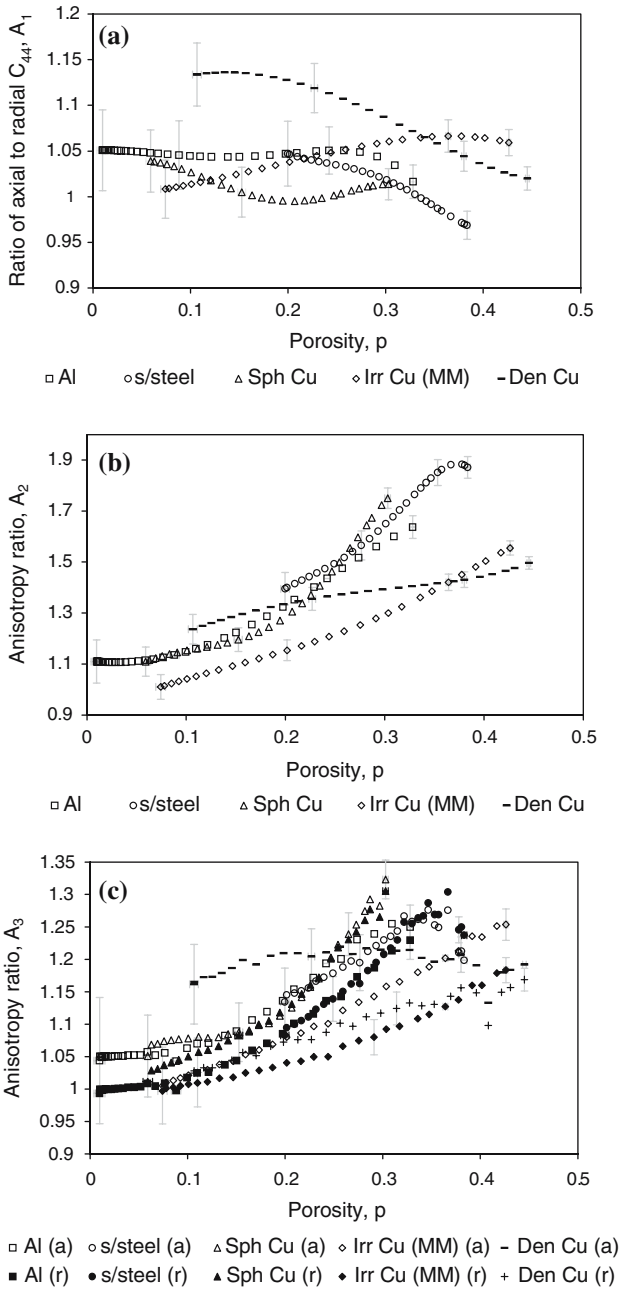

Fig. 2 Elastic anisotropy of powders during compaction. (**a**) A_1. (**b**) A_2. (**c**) A_3. In all cases, deviations from unity indicate greater anisotropy, see Eqs. 4–6. (□) Aluminium; (○) stainless steel; (Δ) spheroidal copper; (◇) irregular copper (MM); (–) dendritic copper. In (**c**), the open symbols represent A_3 calculated using $C_{44,\ \mathrm{axial}}$, while for the filled symbols $C_{44,\ \mathrm{radial}}$ was used. (+) represents A_3 for the dendritic copper powder calculated using $C_{44,\ \mathrm{radial}}$

measurement did not match that of the axial shear wave speed measurement.

By itself, agreement between $C_{44,\ \mathrm{axial}}$ and $C_{44,\ \mathrm{radial}}$ demonstrates that the powder is either transversely or completely isotropic during compaction. To distinguish

between the two possibilities, other measures of anisotropy, such as those defined in Eqs. 5 and 6, are required (Fig. 2b, c). As the wave speed data alluded, these ratios show compressive anisotropy (A_2) is more pronounced than shear anisotropy (A_3). Again, both indicate decreasing anisotropy as porosity approaches zero. Given pores are expected to become increasingly spheroidal as solid phase density is approached, this suggests pore anisotropy dominates anisotropy induced by preferred orientation of the solid phase crystal structure during compaction. The possibility this result is due to counter-balancing effects of pore and crystalline anisotropy is considered unlikely, as the level of elastic anisotropy for the spheroidal copper and aluminium powders is similar despite elastic anisotropy of the copper crystal structure being approximately 2.5 times that of aluminium [38].

With elastic anisotropy of the powders during uniaxial compaction firmly established, the isotropic elastic moduli as calculated by Eqs. 1 and 2 are unsuitable for characterising the elastic properties of powder undergoing uniaxial compaction. As discussed previous, description of the compact as a transversely isotropic medium appears most appropriate given the prevailing compaction geometry. Experimental data considered just prior supports this.

Five elastic moduli are required to describe the elastic response of a transversely isotropic medium. The five independent components of the stiffness matrix (C_{11}, C_{12}, C_{33}, C_{13}, C_{44}) can be re-cast into a form closer to the 'engineering moduli' (E, v, μ, k, etc.), by considering the inverse of the generalised Hooke's law (Eq. 3).

$$\varepsilon_i = S_{ij}\sigma_j \tag{7}$$

with S_{ij} the elastic compliances (the inverse of C_{ij}). Expanding gives (for transverse isotropy):

$$\begin{bmatrix} \varepsilon_{11} \\ \varepsilon_{22} \\ \varepsilon_{33} \\ \varepsilon_{23} \\ \varepsilon_{31} \\ \varepsilon_{12} \end{bmatrix} = \begin{bmatrix} S_{11} & S_{12} & S_{13} & 0 & 0 & 0 \\ S_{12} & S_{11} & S_{13} & 0 & 0 & 0 \\ S_{13} & S_{13} & S_{33} & 0 & 0 & 0 \\ 0 & 0 & 0 & S_{44} & 0 & 0 \\ 0 & 0 & 0 & 0 & S_{44} & 0 \\ 0 & 0 & 0 & 0 & 0 & S_{66} \end{bmatrix} \begin{bmatrix} \sigma_{11} \\ \sigma_{22} \\ \sigma_{33} \\ \sigma_{23} \\ \sigma_{31} \\ \sigma_{12} \end{bmatrix}$$

$$\begin{bmatrix} \varepsilon_{11} \\ \varepsilon_{22} \\ \varepsilon_{33} \\ \varepsilon_{23} \\ \varepsilon_{31} \\ \varepsilon_{12} \end{bmatrix} = \begin{bmatrix} \frac{1}{E_r} & \frac{-v_r}{E_r} & \frac{-v_a}{E_a} & 0 & 0 & 0 \\ \frac{-v_r}{E_r} & \frac{1}{E_r} & \frac{-v_a}{E_a} & 0 & 0 & 0 \\ \frac{-v_a}{E_a} & \frac{-v_a}{E_a} & \frac{1}{E_a} & 0 & 0 & 0 \\ 0 & 0 & 0 & \frac{1}{\mu_a} & 0 & 0 \\ 0 & 0 & 0 & 0 & \frac{1}{\mu_a} & 0 \\ 0 & 0 & 0 & 0 & 0 & \frac{1}{\mu_r} \end{bmatrix} \begin{bmatrix} \sigma_{11} \\ \sigma_{22} \\ \sigma_{33} \\ \sigma_{23} \\ \sigma_{31} \\ \sigma_{12} \end{bmatrix} \tag{7a}$$

Thus, five elastic moduli can be defined for the transversely isotropic medium, which are closely analogous to the elastic moduli for an isotropic medium [14]. Their relation with the moduli C_{ij} are as given by Eq. 8.

$$\begin{aligned} E_r &= \frac{1}{S_{11}} = \frac{(C_{11}-C_{12})\left(C_{11}C_{33}+C_{12}C_{33}-2C_{13}^2\right)}{C_{11}C_{33}-C_{13}^2} \\ E_a &= \frac{1}{S_{33}} = \frac{\left(C_{11}C_{33}+C_{12}C_{33}-2C_{13}^2\right)}{C_{11}+C_{12}} \\ \mu_r &= \frac{1}{S_{66}} = \frac{1}{2}(C_{11}-C_{12}) \\ \mu_a &= \frac{1}{S_{44}} = C_{44} \\ v_r &= \frac{-S_{12}}{S_{11}} = \frac{C_{12}C_{33}-C_{13}^2}{C_{11}C_{33}-C_{13}^2} = \frac{E_r}{2\mu_r} - 1 \\ v_a &= \frac{-S_{13}}{S_{33}} = \frac{C_{13}}{C_{11}+C_{12}} \end{aligned} \tag{8}$$

E_r is Young's modulus of the radial plane, and likewise E_a is Young's modulus for the axial plane. v_a represents strain in the radial direction resulting from stress applied in the axial direction, while v_r determines strain in a radial direction due to stress applied in a different radial direction, perpendicular to the strain direction. μ_a is the shear modulus of planes parallel to the axial direction; μ_r the shear modulus of the radial plane. Importantly though, in the absence of data on C_{13}, neither E_a, E_r, v_a, or v_r can be calculated. However, these quantities can be estimated by use of the *Saint-Venant approximation* (e.g. [39, 40]).

$$\frac{1}{\mu_a} = \frac{1}{E_r} + \frac{2v_a+1}{E_a} \tag{9}$$

This is an empirical relation. However, in a survey of experimental data on different types of anisotropic rocks, Worotnicki [39] has shown Eq. 9 to be widely, although not universally applicable. Support for applying this relation in the present case, can also be drawn from the behaviour of models used to predict elastic properties of porous materials. Model equations for the elastic properties of anisotropic bodies containing non-interacting cavities suggested by Shafiro and Kachanov [41], can be reduced to Eq. 9. Likewise, within the scope of a model for the elastic properties of porous materials suggested by Zhao et al. [42], Eq. 9 is satisfied to within 15% (see [10, Hentschel and Page submitted] for a discussion of this model). Further, a model for the elastic moduli of a hexagonal close-packed array of identical spheres by Duffy [43] satisfies

Eq. 9 to within a maximum of 6%. While these results certainly provide encouragement for the validity of the Saint-Venant approximation, it must be acknowledged that rigorous experimental justification is still lacking.

Adopting the Saint-Venant approximation, an estimate of C_{13} can be obtained combining Eqs. 8 and 9. After some minor simplifications, Eq. 10 results.

$$C_{44} = \frac{(C_{11} - C_{12})\left(C_{11}C_{33} + C_{12}C_{33} - 2C_{13}^2\right)}{\left(C_{11}C_{33} - C_{13}^2\right) + (C_{11} - C_{12})(2C_{13} + C_{11} + C_{12})} \quad (10)$$

As explicit solution to obtain C_{13} as a function of the four remaining components of the stiffness matrix is mathematically complex, a numerical solution was implemented. The resulting estimates of C_{13}, along with measured values of C_{11}, C_{12}, C_{33}, and C_{44} allows calculation of elastic moduli for the axial and radial planes (i.e. E_a, E_r, ν_a, ν_r, μ_a, μ_r) as defined in Eq. 8. These moduli are presented in Fig. 3 as a function of porosity during compaction. In order to facilitate comparison between different material types, shear and Young's modulus values for each different material

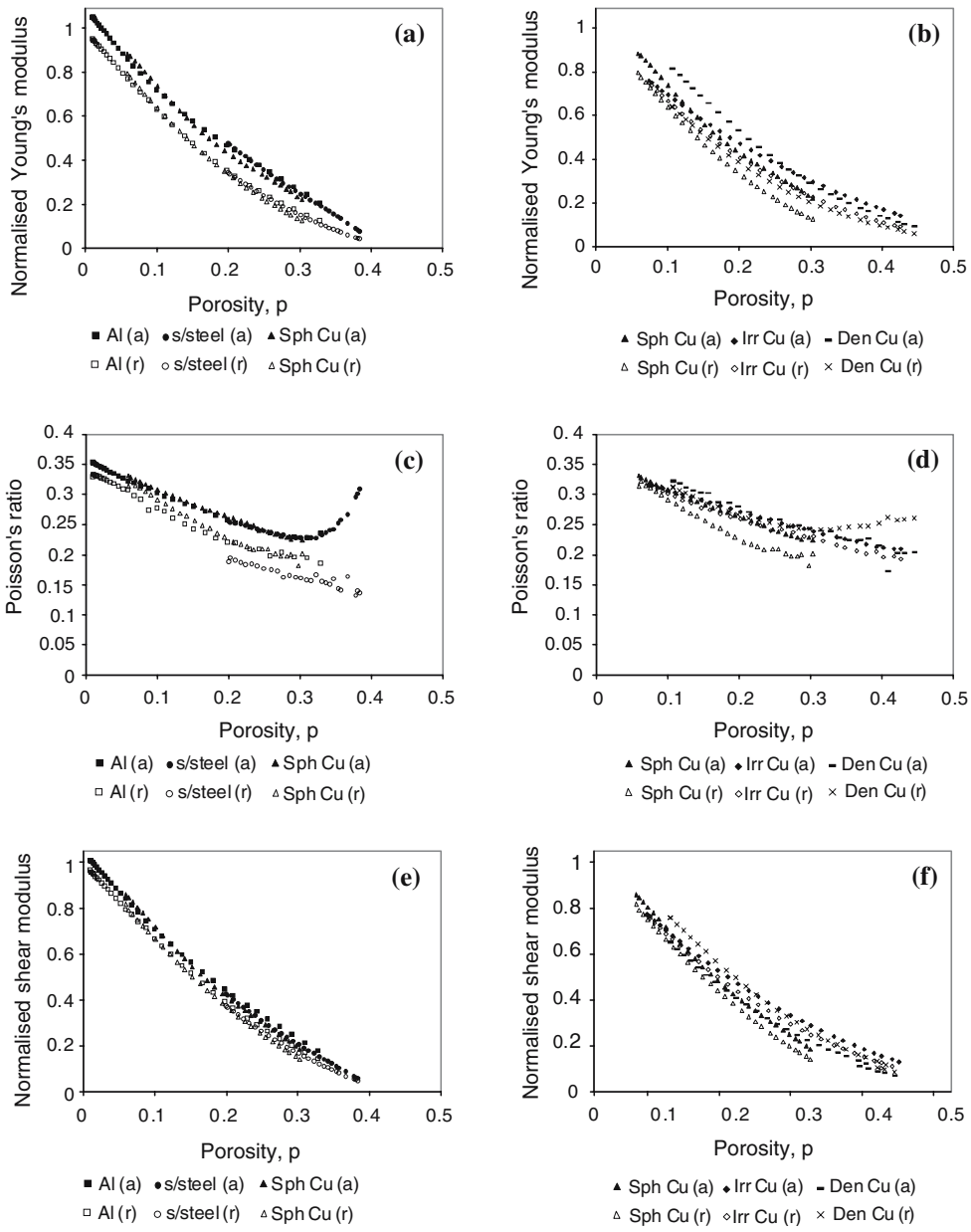

Fig. 3 Comparison between estimates of elastic moduli for radial and axial planes. (**a**, **b**) Young's modulus. Values have been normalised by the appropriate isotropic solid phase Young's modulus for each material: 67.6, 195, 115 GPa for aluminium, stainless steel, and copper respectively. (**c**, **d**) Poisson's ratio. (**e**, **f**) shear modulus normalised by solid phase values: 25, 75.6, 42.6 GPa for aluminium, stainless steel, and copper respectively. (□) Aluminium; (○) stainless steel; (Δ) spheroidal copper; (◇) irregular copper; (–) dendritic copper, values for axial plane (×) dendritic copper values for radial plane. For other powders, open symbols correspond to the radial plane, and filled symbols to the axial plane. Note that only five of the six moduli shown are independent

are normalised by their respective solid phase values for an isotropic material. It is felt that this normalisation procedure is justified by the observed approach towards isotropy exhibited by each compact. However, it is noted that this may not be appropriate method if compaction were to generate significant preferred orientation of a crystal structure with high elastic anisotropy. For example, measurements on compacted graphite powder described by Krzesińska et al. [32], would be most appropriately normalised by the corresponding crystalline values of elastic moduli, rather than the isotropic values (which are an average over all crystalline directions). Results for the five different powders are separated in two groups, illustrating effects of solid phase elastic properties (spheroidal powders in Fig. 3a, c, e), and pore character (different shaped copper powders in Fig. 3b, d, f) respectively.

This figure yields some interesting points. First, each elastic modulus is higher in the axial plane than for the radial plane, consistent with the wave speed results discussed earlier. Second, for a given plane (axial or radial), the influence of particle material and particle shape on Young's, modulus and Poisson's ratio is similar to results discussed in a companion paper (Hentschel and Page submitted). For example, considering Young's modulus of the radial plane, data for the three spheroidal metal powders closely coincides when normalised by respective solid phase values. Thus, the variation of Young's modulus with porosity in the radial plane is also accounted for by solid phase elastic properties. With regard to the effects of particle shape, each of the moduli shows similar qualitative behaviour to the moduli calculated from axial wave speeds and assuming elastic isotropy (*pseudo-isotropic moduli*) in Hentschel and Page (submitted). Again, a more rugged particle shape produces compliant compacts. The physical basis of this response can be interpreted in the same manner as described in Hentschel and Page (submitted).

Finally, and perhaps most importantly, the results of Fig. 3 show the qualitative dependence of the axial plane moduli is similar to the evolution with porosity presented in Hentschel and Page (submitted). This result provides support for data presented in Hentschel and Page (submitted), indicating that despite the presence of anisotropy, axial wave speeds provide a useful measure of Young's modulus and Poisson's ratio for the axial plane.

Conclusions

Elastic wave speeds have been measured in powders undergoing uniaxial compaction. Comparison between in situ wave speed measurements in the axial (pressing) and radial directions shows the powder compact exhibits significant elastic anisotropy. This was attributed to corresponding anisotropies in pore character induced during compaction. Elastic anisotropy was found to be most pronounced mid-way through compaction; at the highest and lowest porosities, wave speeds appear to be convergent, indicating elastic isotropy.

In general, the compact was best described as a transversely isotropic medium, requiring five moduli to characterise its elastic behaviour. From the wave speed data measured, four of these moduli were calculated directly. Utilising the Saint-Venant approximation, these were then cast into a form analogous to the isotropic engineering elastic moduli (Young's modulus, Poisson's ratio, shear modulus, etc.). Moduli for the axial plane were found to be qualitatively similar to analogous pseudo-isotropic elastic moduli, which were calculated from axial wave speed data only with the assumption of elastic isotropy. Solid phase elastic properties, and particle shape were found to affect the transversely isotropic elastic moduli in a manner similar to that found for the pseudo-isotropic moduli discussed elsewhere (Hentschel and Page submitted).

Acknowledgements The authors gratefully acknowledge scholarship support for MLH through the Australian Research Council Small Grants Scheme.

References

1. German RM (1994) Powder metallurgy science, 2nd edn. Metal Powder Industries Federation, New Jersey
2. Özkan N, Briscoe BJ (1997) Ceram Int 23:521
3. Özkan N, Briscoe BJ (1997) J Eur Ceram Soc 17:697
4. Deis TA, Lannutti JL (1998) J Am Ceram Soc 81:1237
5. Rajab M, Coleman DS (1985) Powder Metall 28:207
6. Thompson RA (1981) Ceram Bull 60:237
7. Liu C-H, Nagel SR, Schecter DA, Coppersmith SN, Majumdar S, Narayan O, Witten TA (1995) Science 269:513
8. Rice RW, Donahue TJ (1979) J Am Ceram Soc 62:306
9. Dawson ALeR, Piché L, Hamel A (1996) Powder Metall 39:275
10. Hentschel ML (2002) PhD thesis, The University of Newcastle
11. Meyers MA (1994) Dynamic behaviour of materials. Wiley, New York
12. Love AEH (1944) A treatise on the mathematical theory of elasticity, 4th edn. Dover, New York
13. Timoshenko SP, Goodier JN (1982) Theory of elasticity, 3rd edn. McGraw-Hill, Singapore
14. Boresi AP, Schmidt RJ, Sidebottom OM (1993) Advanced mechanics of materials, 5th edn. Wiley, New York
15. Hardin BO, Blandford GE (1989) J Geotech Engng 115:788
16. Matikas TE, Kapur P, Shamasundar S (1997) J Mater Sci 32:1099

17. Jones MP, Blessing GV (1988) In: McGonnagle WJ (ed) International advances in nondestructive testing, vol 13. Gordon & Breach, New York, p 175
18. Kathrina T, Rawlings RD (1997) J Eur Ceram Soc 17:1157
19. Carnavas PC, Page NW (1998) J Mater Sci 33:4647
20. Jones MP, Blessing GV (1987) In: Proceedings of 1987 IEEE ultrasonics symposium, vol 1186, p 587
21. Kendall K (1990) Br Ceram Trans 89:211
22. Denny PJ (2002) Powder Technol 127:162
23. Briscoe BJ, Rough SL (1998) Colloids Surfaces A 137:103
24. Reed JS (1995) Principles of ceramic processing, 2nd edn. Wiley, New York
25. Rice RW (1998) Porosity of ceramics. Marcel Dekker, New York
26. Scarlett B, Van Der Kraan M, Janssen RJM (1998) Philos Trans R Soc Lond Ser A 356:2623
27. Shima S, Saleh MAE (1993) J Am Ceram Soc 76:1303
28. Boccaccini AR (1993) J Mater Sci Lett 12:43
29. Zavaliangos A, Bouvard D (2000) Int J Powder Metall 30:58
30. Martin LP, Nagle D, Rosen M (1998) Mater Sci Eng A 246:151
31. Parthasarathi S, Prucher T (1993) In: Proceedings of the 3rd international conference on powder metallurgy in aerospace, defence, and demanding applications, February 1993, p 75
32. Krzesiñska M, Celzard A, Marêché JF, Puricelli S (2001) J Mater Res 16:606
33. Patterson BR, Miljus KL, Knoop WV (1984) Metal Powder Report 39:145
34. Laughton AS (1957) Geophysics 22:233
35. Brettell JM (1990) J App Phys D 23:620
36. Kupperman DS, Karplus HB (1984) Ceram Bull 63:1505
37. Bućko MM, Haberko K (1999) J Mater Sci 34:6157
38. Mason WP (1958) Physical acoustics and the properties of solids. Van Nostrand, New Jersey
39. Worotnicki G (1993) In: Hudson JA (ed) Comprehensive rock engineering: principles, practice, and projects. Vol 3, Rock testing and site characterisation. Pergamon, Oxford
40. Amadei R (1996) Int J Rock Mech Min Sci Geomech Abstr 33:293
41. Shafiro B, Kachanov M (1999) J Mech Phys Solids 47:877
42. Zhao YH, Tandon GP, Weng GJ (1989) Acta Mech 76:105
43. Duffy J (1959) Trans ASME J Appl Mech 25:88